Article

Parameters of the Electrical Equivalent Model of the Solar Cell

Ahmed Kotbi [1*], Ilham Hamdi Alaoui [1], Bouchaib Hartiti [2], Mohamed Rafi [3], Andreas Zeinert [1], Abderraouf Ridah [4] and Mustapha Jouiad [1*]

[1] Laboratory of Condensed Matter Physics, University of Picardie Jules Verne, 33 Rue Saint Leu, 80039 Amiens, France; ahmed.kotbi@u-picardie.fr (A.K.); ilham.hamdi.alaoui@u-picardie.fr (I.H.A.); andreas.zeinert@u-picardie.fr (A.Z.) ; mustapha.jouiadt@u-picardie.fr (M.J.)
[2] Laboratory LVOBEEN, GMEEM&DD Group, Hassan II University of Casablanca, FSTM, BP 146, 2065, Mohammedia, Morocco (B.H.)
[3] Industrial Engineering Lab, Mohammed VI International Academy of Civil Aviation, 27000 Casablanca, Morocco; mohamed.rafi@aiac.ma (M.R.)
[4] LIMAT Lab, Faculty of Sciences Ben M'sick, Hassan II University, 7955 Casablanca, Morocco; abderraouf.ridah@univh2c.ma (A.R.)
* Correspondence: mustapha.jouiad@u-picardie.fr (M.J.); ahmed.kotbi@u-picardie.fr (A.K.); Tel.: +33 3-22-82-78-27

Abstract: We report on two analytical methods describing the electrical properties of photovoltaic modules. The improved nonlinear five-point model (INFP) and the least squares (LS) method were evaluated in terms of the efficacy in determining the intrinsic parameters of photovoltaic modules based on silicon technology both monocrystalline and polycrystalline. The INFP model, used to replicate the electrical behavior of photovoltaic modules, is generally based on simplified assumptions that provide a practical mathematical framework. We leveraged the advantages of the LS method to better account for diode effects and nonlinear behaviors. To assess the ability of the two methods to adapt to different photovoltaic technologies, we evaluated these methods on two distinct technologies under variable irradiation levels. Our findings were further compared to the manufacturers published data. The least squares method is convenient and fast, but it may lack the precision of more rigorous analytical methods such as the five-point method. Subsequently, both INFP and LS models were applied to our processed solar cell based on n-SnS_2/p-Si and perovskite, which showed their capabilities to extract intrinsic parameters towards small thin-film cells with low photovoltaic efficiency.

Keywords: Photovoltaic; modules; silicon technology; diode effects; n-SnS_2/p-Si

1. Introduction

Various methods have been developed to predict the performance of photovoltaic (PV) modules (Farah et al. 2022; Vais et al. 2023). Most of these approaches rely on an equivalent electrical circuit, usually represented in its simplest form as a current source in parallel with a diode, modeling the P-N junction (Ibrahim and Anani 2017). The advanced models integrated additional parasitic elements, such as series and shunt resistors, to improve the simulations accuracy. Multi-diodes configuration further refined the modeling of P-N junctions in PV devices, achieving higher accuracy at the expense of an increased computational complexity (Izci et al. 2024). Given the nonlinear nature of the current-voltage (I-V) relationship in PV modules, determining the PV device parameters require substantial computational effort. Analytical techniques can determine each parameter individually under specific constraints, while other methods extract multiple parameters simultaneously using algebraic equations (Ghetas and Elshourbagy 2024; Maniraj and Peer Fathima 2020). Iterative approaches leveraging artificial intelligence (AI) methodologies, such as fuzzy logic (FL) and artificial neural networks (ANN) (Ali et al. 2021; Celik 2011; El-Sehiemy et al. 2023; Fathi and Parian 2021; Garud et al. 2021; Sarang et al. 2024), have also been explored to optimize these calculations. When applying these parameter extraction methods to PV modules, the following assumptions were considered: all connected cells are identical and exposed to uniform irradiance and temperature conditions, the short-circuit current is assumed to be equal to the photocurrent and directly depends on the solar radiation intensity, and the voltage drops on the interconnected conductors are negligible.

Extracting the current-voltage (I-V) characteristics of photovoltaic cells and their tandem configurations is essential to evaluate their performance. Various experimental and modeling approaches allow determining these characteristics while taking into account optical, electronic, and thermal effects. Tunable illumination

acquisition techniques (Lehr et al. 2020) and numerical modeling are used to analyze the internal electrical parameters. The influence of optoelectronic effects, such as recombination at interfaces, is crucial to understand the behavior of tandem cells (Langenhorst et al. 2019). The impact of parasitic resistances on performance is discussed in the study by (Montes-Romero et al. 2018), while the optimization of charge transport at interfaces is explored by (Arnaoutakis et al. 2022).

This study proposes to use a single-diode model, which provides a balance between efficiency and computational accuracy, to identify PV key parameters such as the photocurrent (I_{ph}), the saturation current (I_s), the ideality factor (A), and the parasitic series (R_s) and shunt (R_{sh}) resistances. We aim then to introduce an improved methodology to characterize PV systems using both the classical five-point model and the least-squares method and provide comparative study while considering non-ideal diode characteristics and nonlinear effects.

The materials used in solar panels play a crucial role in their efficiency. Traditional silicon-based solar cells, which convert solar energy into electricity, have a recorded efficiency of 23%. However, they are costly and have relatively low efficiency. Researchers are exploring ways to enhance solar cell performance, particularly by developing perovskite solar cells (Huang et al. 2025; Khatoon et al. 2023). These cells achieve a higher efficiency of 31% compared to the 18% efficiency of conventional solar cells (Sriabisha and Hariharan 2020; Teixeira et al. 2022). Despite their potential, perovskite cells face challenges such as instability and the presence of water-soluble lead. This article analyzes silicon-based cells, perovskite cells, and thin-film cells used in solar panels.

2. Theory and Analysis

An ideal PV module consists of a single diode connected in parallel with a light-generated current source (I_{ph}). The current-voltage (I-V) relationship follows a simple Shockley-type exponential characteristic with an ideality factor. However, a real PV module incorporates both series (R_s) and shunt (R_{sh}) resistances to account for internal losses (see Figure 1). Series resistance represents the resistive losses within the solar cell and its electrical connections. It includes the resistance of the front and back contacts, as well as interconnection losses in the case of a module, while shunt resistance models the leakage current across the junctions. The output current equation for such a module can be expressed as follows:

$$I = I_{ph} - I_s\left(exp\left(\frac{V + IR_s}{nV_{th}}\right) - 1\right) - \frac{V + IR_s}{R_{sh}} \quad (1)$$

where n is the ideality factor, I_s is the saturation current, the thermal voltage is defined as $V_{th} = KT_c/q$, where K is the Boltzmann constant, T_c is the cell temperature, and q is the elementary charge.

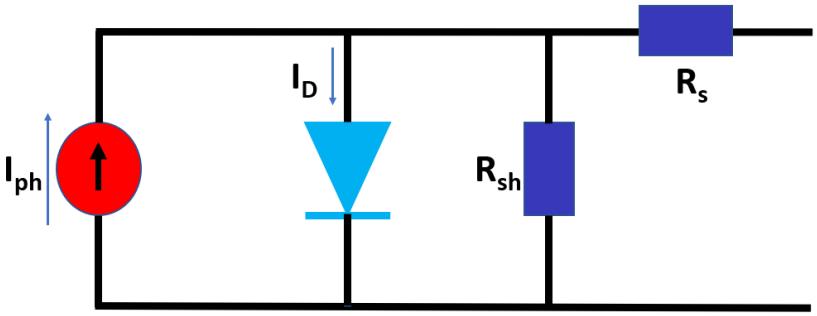

Figure 1. PV circuit model with series and parallel resistances

2.1. Nonlinear Five-Point Model

The five-point model is an analytical approach used to derive device parameters from the measured values of key operational quantities at specific points on the I-V curve. These points include the open-circuit voltage (V_{oc}), short-circuit current (I_{sc}), voltage at the maximum power point (V_m), current at the maximum power point (I_m), the slope at the open-circuit point (R_{s0}), and the slope at the short-circuit point (R_{sh0}) (Bogning Dongue et al. 2013a).

In this study, the parameters were determined through correlations involving the current and voltage at critical operational points: the short-circuit point, the open-circuit point, and the maximum power point (MPP). These correlations provide three independent equations, as represented in (2)–(4).

At short-circuit point, $V = 0$, $I = I_{sc}$:

$$I_{sc} - I_{ph} + I_s\left(exp\left(\frac{I_{sc}R_s}{nV_{th}}\right) - 1\right) + \frac{I_{sc}R_s}{R_{sh}} = 0 \quad (2)$$

At the open-circuit point, $I = 0$, $V = V_{oc}$:

$$-I_{ph} + I_s\left(exp\left(\frac{V_{oc}}{nV_{th}}\right) - 1\right) + \frac{V_{oc}}{R_{sh}} = 0 \quad (3)$$

At maximum power point MPP, $I=I_m$,$V=V_m$:

$$I_m - I_{ph} + I_s\left(exp\left(\frac{V_m + I_mR_s}{nV_{th}}\right) - 1\right) + \frac{V_m + I_mR_s}{R_{sh}} = 0 \quad (4)$$

The derivation of equation (1) at $V = V_{oc}$:

$$\left(\frac{dV}{dI}\right)_{V=Voc} = \frac{1 + R_s\left(\frac{I_s}{nV_{th}}exp\left(\frac{V_{oc}}{nV_{th}}\right) + \frac{1}{R_{sh}}\right)}{-\frac{I_s}{nV_{th}}exp\left(\frac{V_{oc}}{nV_{th}}\right) - \frac{1}{R_{sh}}} = -R_{s0} \quad (5)$$

The derivation of equation (1) at $I = I_{sc}$:

$$\left(\frac{dV}{dI}\right)_{I=Isc} = \frac{1 + R_s\left(\frac{I_s}{nV_{th}}exp\left(\frac{I_{sc}R_s}{nV_{th}}\right) + \frac{1}{R_{sh}}\right)}{-\frac{I_s}{nV_{th}}exp\left(\frac{I_{sc}R_s}{nV_{th}}\right) - \frac{1}{R_{sh}}} = -R_{sh0} \quad (6)$$

where R_{s0} is the derivative of V as a function of I at the open circuit point, and R_{sh0} is the derivative of V as a function of I at the short circuit point. In this work, R_{s0}, R_{sh0}, V_{oc}, I_{sc}, I_m, V_m are determined experimentally and injected into the system of equations.

From equation (3) we obtain the expression of the photoelectric I_{ph} and we replace it in equation (2) and (4), after some mathematical manipulations, we then obtain the following system equations with four parameters:

$$I_s\left(exp\left(\frac{V_{oc}}{nV_{th}}\right) - exp\left(\frac{I_{sc}R_s}{nV_{th}}\right)\right) - I_{sc}\left(1 + \frac{R_s}{R_{sh}}\right) + \frac{V_{oc}}{R_{sh}} = 0 \quad (7)$$

$$I_m - I_s\left(exp\left(\frac{V_{oc}}{nV_{th}}\right) - exp\left(\frac{V_m + I_mR_s}{nV_{th}}\right)\right) + \frac{V_m + I_mR_s}{R_{sh}} - \frac{V_{oc}}{R_{sh}} = 0 \quad (8)$$

$$(R_{s0} - R_s)\left(\frac{1}{R_{sh}} + \frac{I_s}{nV_{th}}exp\left(\frac{V_{oc}}{nV_{th}}\right)\right) - 1 = 0 \quad (9)$$

$$\frac{1}{R_{sh}} - \frac{1}{R_{sh0} - R_s} + \frac{I_s}{nV_{th}}exp\left(\frac{I_{sc}R_s}{nV_{th}}\right) = 0 \quad (10)$$

The approximations used are given as follows:

$$exp\left(\frac{V_{oc}}{nV_{th}}\right) \gg exp\left(\frac{I_{sc}R_s}{nV_{th}}\right) \quad (11)$$

$$R_{sh} \gg R_s \quad (12)$$

$$\frac{1}{R_{sh}} \ll \frac{I_s}{nV_{th}}exp\left(\frac{V_{oc}}{nV_{th}}\right) \quad (13)$$

$$\frac{I_s}{nV_{th}}exp\left(\frac{I_{sc}R_s}{nV_{th}}\right) \approx 0 \quad (14)$$

The approximations given by equations (11), (13), and (14) are based on physical considerations that simplify the electrical model of the solar cell under standard operating conditions. The approximation formulated by equation (11) indicates that the losses related to metal contacts and interconnections between the cells in a module are minimal. Equation (13) shows that our cell has a high shunt resistance (R_{sh}), meaning that the leakage current through the shunt path is minimal. This indicates a well-manufactured solar cell with negligible recombination losses through these parasitic paths. The approximation in equation (14) assumes that the impact of the series resistance (R_s) on the diode current under short-circuit conditions is negligible. It is based on the fact that $I_{sc}R_s \ll nV_{th}$, meaning that the voltage drop across R_s is small compared to the thermal voltage. Using these approximations, we can find an analytical expression for each of the five parameters, setting $A=nV_{th}$:

$$A = \frac{V_m + I_m R_{s0} - V_{oc}}{ln\left(I_{sc} - \frac{V_m}{R_{sh}} - I_m\right) - ln\left(I_{sc} - \frac{V_{oc}}{R_{sh}}\right) + \frac{I_m}{I_{sc} - \frac{V_{oc}}{R_{sh}}}} \quad (15)$$

$$I_s = \left(I_{sc} - \frac{V_{oc}}{R_{sh}}\right) exp\left(\frac{-V_{oc}}{nV_{th}}\right) \quad (16)$$

$$R_s = R_{s0} - \frac{nV_{th}}{I_0} exp\left(\frac{-V_{oc}}{nV_{th}}\right) \quad (17)$$

$$R_{sh} = R_{sh0} \quad (18)$$

$$I_{ph} = I_{sc}\left(1 + \frac{R_s}{R_{sh}}\right) + I_s\left(exp\left(\frac{I_{sc}R_s}{nV_{th}}\right) - 1\right) \quad (19)$$

2.2. Least Squares Method

This method includes the presentation I=f(V) of the standard function (1) in the form V=f(I) and the determination of the factors C_0, C_1 and C_2 of this function from which the parameters of the illuminated solar cell are evaluated. Starting from equation (1) which can be written in the form:

$$I = \frac{I_{ph} - I_s\left(exp\left(\frac{V + IR_s}{nV_{th}}\right) - 1\right) - G_{sh}V}{1 + G_{sh}R_s} \quad (20)$$

where, $G_{sh}=1/R_{sh}$. The previous equation can also be written:

$$I = I_{pA} - I_0\left(exp\left(\frac{V + IR_s}{nV_{th}}\right) - 1\right) - G_A V \quad (21)$$

where:

$$I_{pA} = \frac{I_{ph}}{1 + G_{sh}R_s} \quad (22)$$

$$I_0 = \frac{I_s}{1 + G_{sh}R_s} \quad (23)$$

$$I_A = \frac{G_{sh}}{1 + G_{sh}R_s} \quad (24)$$

For low and negative bias voltages where the behavior of the I=f(V) curve is linear, the exponential part is negligible and equation (21) can be written in the form:

$$I = I_{pA} - G_A V \quad (25)$$

G_A and I_{pA} are therefore evaluated from (25) by a simple linear regression. The calculated value of G_A gives the product ($G_A V$) which can be added to the measured current. We obtain the corrected current through the solar cell which is given by:

$$I_c = I + G_A V \tag{26}$$

For sufficiently large forward voltages, where the behavior of the I=f(V) curve is exponential, the current through the cell is given by:

$$I_c = I_{pA} + I_0 \left(exp\left(\frac{V + IR_s}{nV_{th}}\right) - 1 \right) \tag{27}$$

To evaluate the series resistance Rs, the ideality factor n and the saturation current Is, we use I instead of V as an independent variable in equation (26), and we obtain:

$$V = nV_{th} ln\left(\frac{I_{pA}}{I_0}\right) - IR_s + nV_{th} ln\left(1 - \frac{I_c}{I_{pA}}\right) \tag{28}$$

Expression (26) can be presented in the form:

$$V = C_0 + C_1 I + C_2 ln\left(1 - \frac{I_c}{I_{pA}}\right) \tag{29}$$

where:

$$C_0 = nV_{th} ln\left(\frac{I_{pA}}{I_0}\right) \tag{30}$$

$$C_1 = -R_s \tag{31}$$

$$C_2 = nV_{th} \tag{32}$$

The values of the factors C_0, C_1 and C_2 can be obtained from the experimental I-V characteristic of the cell using the least squares method. This results in the following system of equations:

$$\sum_{i=1}^{N} V_i = NC_0 + C_1 \sum_{i=1}^{N} I_i + C_2 \sum_{i=1}^{N} ln\left(1 - \frac{I_{ci}}{I_{pA}}\right) \tag{33}$$

$$\sum_{i=1}^{N} V_i I_i = C_0 \sum_{i=1}^{N} I_i + C_1 \sum_{i=1}^{N} {I_i}^2 + C_2 \sum_{i=1}^{N} I_i ln\left(1 - \frac{I_{ci}}{I_{pA}}\right) \tag{34}$$

$$\sum_{i=1}^{N} V_i ln\left(1 - \frac{I_{ci}}{I_{pA}}\right) = C_0 \sum_{i=1}^{N} ln\left(1 - \frac{I_{ci}}{I_{pA}}\right) + C_1 \sum_{i=1}^{N} I_i ln\left(1 - \frac{I_{ci}}{I_{pA}}\right) + C_2 \sum_{i=1}^{N} ln^2\left(1 - \frac{I_{ci}}{I_{pA}}\right) \tag{35}$$

The given system can be easily solved using Kramer's rule; N is the number of experimental data, (I_i – V_i) are the measured values of current-voltage and I_{ci} is the value of the corresponding corrected current.

$$\begin{pmatrix} \sum_{i=1}^{N} V_i \\ \sum_{i=1}^{N} V_i I_i \\ \sum_{i=1}^{N} V_i ln\left(1 - \frac{I_{ci}}{I_{pA}}\right) \end{pmatrix} = \begin{pmatrix} N & \sum_{i=1}^{N} I_i & \sum_{i=1}^{N} ln\left(1 - \frac{I_{ci}}{I_{pA}}\right) \\ \sum_{i=1}^{N} I_i & \sum_{i=1}^{N} {I_i}^2 & \sum_{i=1}^{N} I_i ln\left(1 - \frac{I_{ci}}{I_{pA}}\right) \\ \sum_{i=1}^{N} ln\left(1 - \frac{I_{ci}}{I_{pA}}\right) & \sum_{i=1}^{N} I_i ln\left(1 - \frac{I_{ci}}{I_{pA}}\right) & \sum_{i=1}^{N} ln^2\left(1 - \frac{I_{ci}}{I_{pA}}\right) \end{pmatrix} \begin{pmatrix} C_0 \\ C_1 \\ C_2 \end{pmatrix} \tag{134}$$

The values of series resistance, ideality factor and current I_0 are determined from the following equations:

$$I_0 = I_{pA} exp\left(\frac{C_0}{C_2}\right) \tag{36}$$

$$R_s = -C_1 \tag{37}$$

$$n = \frac{C_2}{V_{th}} \tag{38}$$

$$G_{sh} = \frac{G_A}{1 - G_A R_s} \tag{39}$$

$$I_{ph} = \frac{I_{pA}}{1 - G_A R_s} \tag{40}$$

$$I_s = \frac{I_0}{1 - G_A R_s} \tag{41}$$

2.3. Preparation of n-SnS_2/p-Si based solar cell

Thin films of SnS_2 were synthesized using a sol-gel method combined with dip coating. The process involved dissolving tin (II) chloride in ethanol to prepare a 0.1 g/mL solution, followed by the dissolution of thiourea in ethanol at a concentration of 0.2 g/mL. These two solutions were then mixed to form the deposition solution. Pre-cleaned P-doped silicon substrates (1×1 cm^2) were immersed in this solution, and the resulting samples were annealed at 300 °C for 10 minutes.

The surface morphology of the films was examined using scanning electron microscopy (SEM), while Raman spectroscopy provided insights into the vibrational modes and confirmed the material's structural properties. UV-Vis spectroscopy was used to analyze the optical properties, including the optical bandgap, and to assess the overall quality of the deposited films. Microstructural analysis was conducted using a Quanta 200 scanning electron microscope from Oxford Instruments. The vibrational properties were studied with a Renishaw micro-Raman spectrometer, utilizing a 532 nm excitation source. Optical properties were characterized using a JASCO V-670 spectrometer equipped with a PIN-757 integrating sphere, operating in both transmission and reflectance modes.

These modules include monocrystalline and polycrystalline silicon technologies, as well as thin-film CIS technology, specifically represented by Shell Monocrystalline SM55 (65.5 cm × 66.8 cm), Shell Polycrystalline S75 (77.5 cm × 66.5 cm), and Shell CIS Thin-film ST40 (33 cm × 129 cm), respectively. The experimental data were extracted from the manufacturer's datasheets (Khezzar et al. 2014; Shell), and the main characteristics of these modules are summarized in Table 1.

Table 1 Data from commercial solar panels for monocrystalline SM55, polycrystalline S75, and CIS thin-film ST40

Parameter	Monocrystalline SM55	Polycrystalline S75	CIS Thin-film ST40
	Five-parameter model (Bogning Dongue et al. 2013b)	Five-parameter model (Bogning Dongue et al. 2013b)	Five-parameter model (Bogning Dongue et al. 2013b)
1000 W/m^2			
I_{ph} (A)	3.453	4.715	2.702
I_s (A)	9.721E−8	9.193E−8	3.463E−7
A	1.338	1.311	1.361
R_s (Ω)	0.3	0.2	1.3
R_{sh} (Ω)	350	179	250
800 W/m^2			
I_{ph} (A)	2.771	3.774	2.157
I_s (A)	5.398E−7	3.961E−7	2.994E−6
A	1.486	1.432	1.571
R_s (Ω)	0.2371	0.1283	1.02
R_{sh} (Ω)	436	223.6	312.5
600 W/m^2			
I_{ph} (A)	2.087	2.832	1.616
I_s (A)	1.624E−6	9.402E−7	13.64E−6

A	1.606	1.519	1.771
R_s (Ω)	0.1762	0.117	0.7465
R_{sh} (Ω)	578.7	297.8	416.7

3. Results

3.1. Photovoltaic modules

The capabilities of the five-point nonlinear model and the least-squares method in predicting the electrical response of photovoltaic (PV) devices has been validated using experimental data obtained from various PV modules (Khezzar et al. 2014; Shell).

Table 2 Parameters for the proposed model for monocrystalline SM55, polycrystalline S75, and CIS thin-film ST40

Parameter	Monocrystalline SM55		Polycrystalline S75		CIS Thin-film ST40	
	Nonlinear Five-Point Model	Least Squares Method	Nonlinear Five-Point Model	Least Squares Method	Nonlinear Five-Point Model	Least Squares Method
1000 W/m²						
I_{ph} (A)	3.374	3.371	4.806	4.814	2.640	2.6542
I_s (A)	1.656E−7	7.993E−8	2.904E−9	3.235E−8	3.374E−7	9.983E−7
A	1.277	1.218	1.0	1.123	1.47	1.58
R_s (Ω)	0.2923	0.2904	0.2251	0.2056	1.3197	1.1832
R_{sh} (Ω)	278.6	269.9	179.6	188.4	265.9	194.8
800 W/m²						
I_{ph} (A)	2.687	2.687	3.8424	3.8485	2.1805	2.1912
I_s (A)	7.941E−8	6.306E−7	1.495E−8	2.469E−10	3.288E−6	1E−6
A	1.2215	1.3791	1.0823	0.8934	1.7082	1.5715
R_s (Ω)	0.2054	0.0794	0.1198	0.323	1.0175	1.1417
R_{sh} (Ω)	418.8492	400	189.9	155.8	241.73	174.29
600 W/m²						
I_{ph} (A)	2.0195	2.0173	2.8811	2.8849	1.6329	1.6492
I_s (A)	1.16E−7	2.589E−8	1.959E−8	1.115E−9	8.974E−6	1.465E−6
A	1.2519	1.1468	1.0965	0.9509	1.848	1.6081
R_s (Ω)	0.1483	0.3682	0.1068	0.2770	0.869	1.1104
R_{sh} (Ω)	566.7	666.29	269.1	256.1	317.45	187.56

By applying the five-point nonlinear model and the least-squares method to the selected PV modules under different irradiance levels, the calculated results were compared to those obtained using the five-parameter model described in (Bogning Dongue et al. 2013b) to assess the accuracy of the proposed approaches (see Table 2). Figure 2 illustrates the I-V characteristic curves evaluated using the proposed models alongside the experimental data provided by the manufacturers. The comparison shows excellent agreement between the I-V curves generated by the proposed models and the experimental data for all module types under various operating conditions.

Notably, the five-point model demonstrates higher accuracy across different levels of irradiance, while the least squares method exhibits better precision at higher irradiance levels. Both models explicitly account for the irradiance dependence of all parameters, which enhances their accuracy. More specifically, the shunt resistance increases with rising irradiance for monocrystalline, polycrystalline, and CIS thin-film modules in both the least squares and five-point methods, same behavior was reported in this work (Kassis and Saad 2010). However, an exception is observed for the CIS thin-film module, where the shunt resistance remains nearly constant when using the least squares method. Conversely, the series resistance decreases as irradiance increases for monocrystalline, polycrystalline, and thin-film modules when applying the five-point method, the same trend was

reported in this work (Shen et al. 2016). A similar trend is observed for CIS thin-film technology when using the least squares method. Additionally, the diode ideality factor increases with higher irradiance levels for CIS thin-film technology in both methods—least squares and five-point—as well as for the polycrystalline module in the five-point method. Table 2 presents the calculated device parameters obtained using both the least squares method and the five-point model at various irradiance levels.

Based on the analysis of these results, the five-point method offers superior accuracy, likely due to its ability to incorporate multiple operating conditions, thereby minimizing the impact of isolated measurement errors. Furthermore, it directly considers the nonlinear effects of cell behavior, making it more reliable for precise modeling. However, this approach also has drawbacks: its implementation is complex due to the need to solve multiple nonlinear equations, often requiring advanced optimization algorithms.

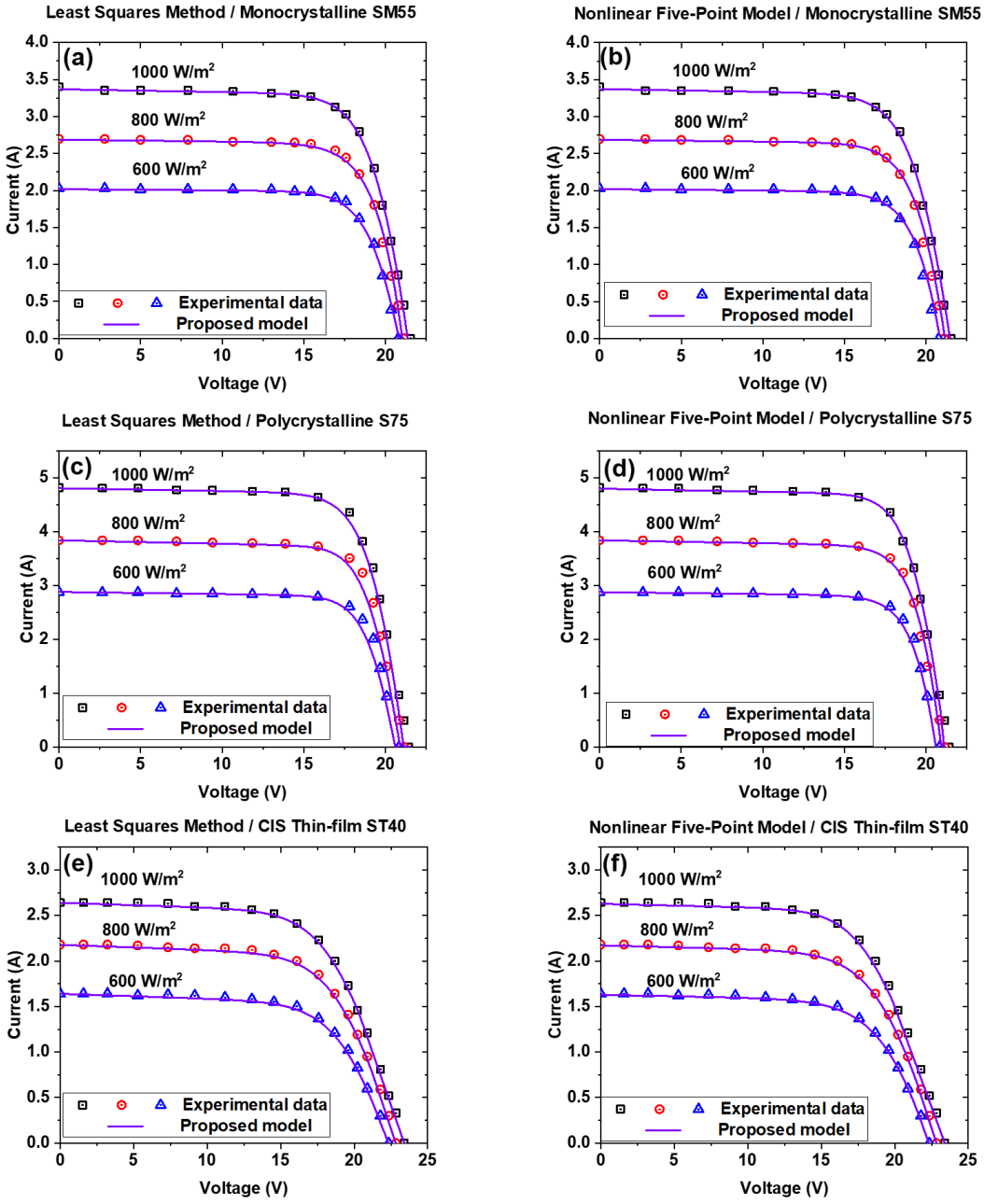

Figure 2. Experimental I-V curves and Calculated curves with Least Squares Method and Nonlinear Five-Point Model for monocrystalline SM55 (a,b), polycrystalline S75 (c,d), and CIS thin-film ST40 (e,f) under varying irradiance levels.

The least squares method is a statistical approach that fits experimental data to extract photovoltaic model parameters. It transforms the model equation into a linear relationship, allowing parameter estimation through linear regression. Its main advantage is its simplicity and speed, as it avoids solving a system of nonlinear equations and can be efficiently applied to large datasets. Additionally, it is easy to implement and does not require specific points on the I-V curve, making it more flexible for experimental data analysis. However, this method also has limitations: it relies on approximations that can reduce the accuracy of extracted parameters, especially for photovoltaic cells with significant nonlinear effects. Furthermore, it is more sensitive to measurement errors, as deviations in the data directly impact the quality of the fit. In summary, the least squares method is practical and fast, but it may lack the precision of more rigorous analytical methods such as the five-point method. A hybrid approach combining both methods could provide a balance between precision and efficiency, optimizing parameter extraction for photovoltaic cells.

3.2. SnS_2 based solar cell

The I-V measurements were also performed on small solar cells based on n-SnS_2/p-Si to assess the ability of the proposed models to determine the intrinsic characteristics of this laboratory-fabricated solar cell.

The SEM image in Figure 3a shows a granular morphology of the SnS_2 material deposited on a P-doped silicon substrate. The grains appear to be micrometer-sized, which could be beneficial for photovoltaic applications. Figure 3b presents the Raman spectrum of a SnS_2 sample at room temperature. The sample exhibits two characteristic peaks of SnS_2: E_2 (~227 cm^{-1}) and A_{1g} (~312 cm^{-1}). The intense peak at approximately 312 cm^{-1} is attributed to the A_{1g} mode, corresponding to the out-of-plane stretching of sulfur atoms in SnS_2 (Wang and Pang 2017; Xiao et al. 2009). The in-plane stretching mode Eg at ~227 cm^{-1} is extremely weak (Smith et al. 1977). These vibrational modes are typical of SnS_2, confirming the presence of this material. An intense peak around 521 cm^{-1} corresponds to silicon (Si), indicating that the underlying substrate is indeed Si.

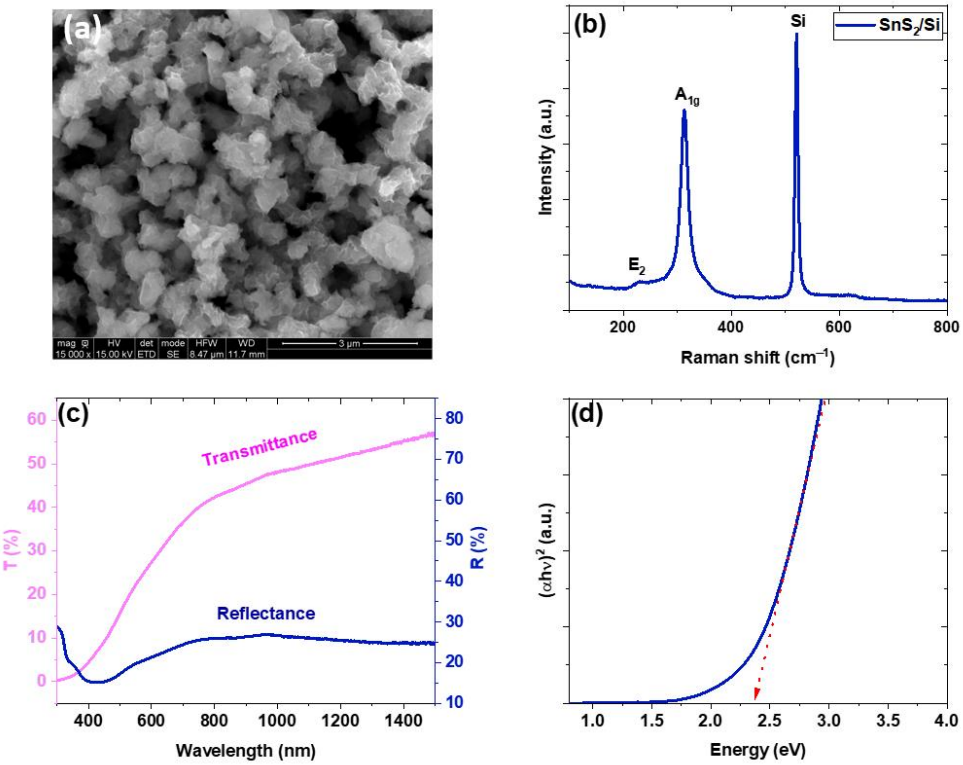

Figure 3. (a) SEM image, (b) Raman spectra, (c) transmittance and reflectance spectra and (d) Tauc plot of SnS_2 thin films.

In Figure 3c, the transmittance increases with wavelength, suggesting that the material is more transparent in the infrared than in the visible range. Reflectance remains relatively low (<20% in the visible), indicating low reflection, which is advantageous for photovoltaic and optical applications. Figure 3d represents $(\alpha h\nu)^2$ as a

function of photon energy hν, allowing the determination of the optical bandgap using Tauc model (Kotbi et al. 2022a; Kotbi et al. 2022b). The linear extrapolation (red dashed line) gives an optical bandgap value of approximately 2.35 eV, which is consistent with SnS_2 (a semiconductor with a bandgap ranging from 2.2 to 2.6 eV) (Burton et al. 2016; Joseph et al. 2020; Zhou and Umezawa 2016). This value suggests that the material is suitable for UV-Vis photodetection and photovoltaic applications.

Figure 4a shows the experimental measurements of the current density as a function of voltage for the n-SnS_2/p-Si photovoltaic cell under different irradiations. The least squares method (purple curve) provides a good approximation of the experimental data, with a globally satisfactory fit. However, it relies on simplifications and may be slightly less accurate at critical points, particularly at high voltage (near V_{oc}). In contrast, the nonlinear five-point model (blue curve) appears to be even more precise, especially in the exponential decay region. It better captures the nonlinear variations in the cell's behavior, making it more faithful to the experimental data. Both models achieve a good fit to the experimental data, but the five-point model seems to offer better accuracy across the entire curve, particularly in the steep slope region. Table 3 summarizes the results obtained from both proposed models. The calculated errors for the two methods, INFP and LS on I-V measurements under 1000W/m², were 7.3×10^{-5} and 3.4×10^{-4}, respectively. This confirms that the five-point nonlinear method is the most accurate. The key parameters of the n-SnS_2/p-Si cell were also extracted for I-V measurements under 1000W/m² irradiation: the open-circuit voltage (V_{oc} =1.22V), the short-circuit current (J_{sc} =3.79 mA), the fill factor (FF=51.21%), and the efficiency (η=2.36%), which is relatively low. This low efficiency is due to the energy barrier between the conduction bands of SnS_2 and p-Si. The proposed models show their capabilities to extract intrinsic parameters towards small thin-film cells with low photovoltaic efficiency.

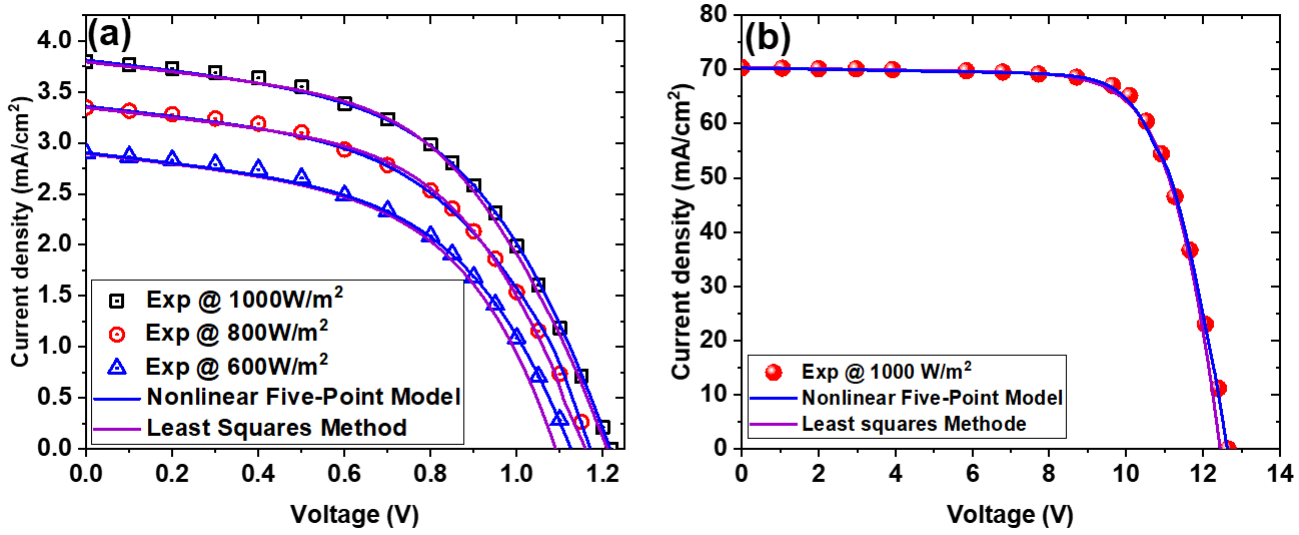

Figure 4. Experimental I-V curves and calculated curves with least squares method and nonlinear five-point Model for (a) n-SnS_2/p-Si thin-film under different irradiations and (b) a Perovskite-based module with an area of 42.9 cm².

Table 3 Parameters for the proposed model for n-SnS_2/p-Si thin-film under varying irradiance levels

Parameter	Nonlinear Five-Point Model	Least Squares Method	Nonlinear Five-Point Model	Least Squares Method	Nonlinear Five-Point Model	Least Squares Method
	1000 W/m²		800 W/m²		600 W/m²	
I_{ph} (mA)	3.91	3.9	3.52	3.5	2.91	2.9
I_s (A)	1.41E−7	1.33E−6	1.03E−6	4.24E−7	3.976E−6	2.11E−6
A	0.12	0.15	0.14	0.13	0.17	0.15
R_s (Ω)	58.55	38.91	45.51	65.88	12.71	30.0
R_{sh} (Ω)	2083.3	2082.3	2145.4	2072.6	2241.6	2117.2

We also performed calculations of the intrinsic parameters of flexible perovskite-based solar cells for a module with a surface area of 42.9 cm^2 (Dai et al. 2020). The calculation results are summarized in Table 4. The two proposed models demonstrate their ability to fit any I-V curve under different irradiations and regardless of the fabrication technology, with higher accuracy using the five-point model. Figure 4b shows the experimental measurements and the fit obtained with both models.

Table 4 Parameters for the proposed model for perovskite solar modules on flexible glass substrates.

Parameter	Nonlinear Five-Point Model	Least Squares Method
	1000 W/m^2	
I_{ph} (mA)	70.4	70.43
I_s (A)	2.19E−11	5.35E−9
A	0.57	0.76
R_s (Ω)	13.93	7.18
R_{sh} (Ω)	8180.7	8783.1

4. Conclusions

In this study, we have analyzed and compared two widely used methods for extracting photovoltaic (PV) model parameters, namely the five-point and the least squares methods. The five-point method offers high precision due to its analytical formulation, relying on characteristic points of the I-V curve to accurately capture the nonlinear behavior of PV cells. In contrast, the least squares method provides a simpler and faster approach, suitable for large datasets and flexible in terms of data requirements. Despite its ease of implementation, it is more sensitive to measurement errors and relies on approximations that may reduce its accuracy in certain conditions. The choice between these methods depends on the specific application: when precision is critical, the five-point method is preferred, whereas the least squares method is ideal for rapid data processing and large-scale analysis. Both proposed models show their capabilities to extract intrinsic parameters also towards small thin-film cells with low photovoltaic efficiency. The errors calculated for the INFP and LS methods were 7.3×10^{-5} and 3.4×10^{-4}, respectively, confirming that the five-point nonlinear method is the most precise.

Author Contributions: Conceptualization, M.J., A.R., B.H. and M.R.; validation, A.K., A.R., M.R.; formal analysis, A.K., A.R.; investigation, A.K., I.H.A and M.R.; data curation, A.K. and I.H.A; visualization, A.R. and R.M. and A.Z.; writing—original draft preparation, A.K.; writing—review and editing, M.J., A.Z., A.R. and M.R., supervision, M.J., A.Z., A.R. and M.R; All authors have read and agreed to the published version of the manuscript.

Funding: This work was supported by PARS (ANR-DFG) project N°22003.

Data Availability Statement: The original contributions presented in the study are included in the article, further inquiries can be directed to the corresponding author.

Conflicts of Interest: The authors declare no conflicts of interest.

References

Ali, M.N., Mahmoud, K., Lehtonen, M., Darwish, M.M.F.: Promising MPPT Methods Combining Metaheuristic, Fuzzy-Logic and ANN Techniques for Grid-Connected Photovoltaic, (2021)

Arnaoutakis, G.E., Favilla, E., Tonelli, M., Richards, B.S.: Single crystal monolithic upconverter solar cell device tandems with integrated optics. J. Opt. Soc. Am. B. 39, 239–247 (2022). https://doi.org/10.1364/JOSAB.437892

Bogning Dongue, S., Njomo, D., Ebengai, L.: A New Strategy for Accurately Predicting I-V Electrical Characteristics of PV Modules Using a Nonlinear Five-Point Model. J. Energy. 2013, 321694 (2013)(a). https://doi.org/https://doi.org/10.1155/2013/321694

Bogning Dongue, S., Njomo, D., Ebengai, L.: An Improved Nonlinear Five-Point Model for Photovoltaic Modules. Int. J. Photoenergy. 2013, 680213 (2013)(b). https://doi.org/https://doi.org/10.1155/2013/680213

Burton, L.A., Whittles, T.J., Hesp, D., Linhart, W.M., Skelton, J.M., Hou, B., Webster, R.F., O'Dowd, G., Reece, C., Cherns, D., Fermin,

D.J., Veal, T.D., Dhanak, V.R., Walsh, A.: Electronic and optical properties of single crystal SnS2: an earth-abundant disulfide photocatalyst. J. Mater. Chem. A. 4, 1312–1318 (2016). https://doi.org/10.1039/C5TA08214E

Celik, A.N.: Artificial neural network modelling and experimental verification of the operating current of mono-crystalline photovoltaic modules. Sol. Energy. 85, 2507–2517 (2011). https://doi.org/https://doi.org/10.1016/j.solener.2011.07.009

Dai, X., Deng, Y., Van Brackle, C.H., Chen, S., Rudd, P.N., Xiao, X., Lin, Y., Chen, B., Huang, J.: Scalable Fabrication of Efficient Perovskite Solar Modules on Flexible Glass Substrates. Adv. Energy Mater. 10, 1903108 (2020). https://doi.org/https://doi.org/10.1002/aenm.201903108

El-Sehiemy, R., Shaheen, A., El-Fergany, A., Ginidi, A.: Electrical parameters extraction of PV modules using artificial hummingbird optimizer. Sci. Rep. 13, 9240 (2023). https://doi.org/10.1038/s41598-023-36284-0

Farah, A., Belazi, A., Benabdallah, F., Almalaq, A., Chtourou, M., Abido, M.A.: Parameter extraction of photovoltaic models using a comprehensive learning Rao-1 algorithm. Energy Convers. Manag. 252, 115057 (2022). https://doi.org/https://doi.org/10.1016/j.enconman.2021.115057

Fathi, M., Parian, J.A.: Intelligent MPPT for photovoltaic panels using a novel fuzzy logic and artificial neural networks based on evolutionary algorithms. Energy Reports. 7, 1338–1348 (2021). https://doi.org/https://doi.org/10.1016/j.egyr.2021.02.051

Garud, K.S., Jayaraj, S., Lee, M.-Y.: A review on modeling of solar photovoltaic systems using artificial neural networks, fuzzy logic, genetic algorithm and hybrid models. Int. J. Energy Res. 45, 6–35 (2021). https://doi.org/https://doi.org/10.1002/er.5608

Ghetas, M., Elshourbagy, M.: Parameters extraction of photovoltaic models using enhanced generalized normal distribution optimization with neighborhood search. Neural Comput. Appl. 36, 14035–14052 (2024). https://doi.org/10.1007/s00521-024-09609-x

Huang, S.-H., Tsou, C.-T., Hsiao, Y.-H., Li, C.-F., Chen, Y.-R., Su, W.-F., Huang, Y.-C.: High-Efficiency Perovskite Solar Cell with an Air-Processable Active Layer via Sequential Deposition. Mater. Sustain. (2025). https://doi.org/10.53941/matsus.2025.100003

Ibrahim, H., Anani, N.: Evaluation of Analytical Methods for Parameter Extraction of PV modules. Energy Procedia. 134, 69–78 (2017). https://doi.org/https://doi.org/10.1016/j.egypro.2017.09.601

Izci, D., Ekinci, S., Hussien, A.G.: Efficient parameter extraction of photovoltaic models with a novel enhanced prairie dog optimization algorithm. Sci. Rep. 14, 7945 (2024). https://doi.org/10.1038/s41598-024-58503-y

Joseph, A., Anjitha, C.R., Aravind, A., Aneesh, P.M.: Structural, optical and magnetic properties of SnS2 nanoparticles and photo response characteristics of p-Si/n-SnS2 heterojunction diode. Appl. Surf. Sci. 528, 146977 (2020). https://doi.org/https://doi.org/10.1016/j.apsusc.2020.146977

Kassis, A., Saad, M.: Analysis of multi-crystalline silicon solar cells at low illumination levels using a modified two-diode model. Sol. Energy Mater. Sol. Cells. 94, 2108–2112 (2010). https://doi.org/https://doi.org/10.1016/j.solmat.2010.06.036

Khatoon, S., Kumar Yadav, S., Chakravorty, V., Singh, J., Bahadur Singh, R., Hasnain, M.S., Hasnain, S.M.M.: Perovskite solar cell's efficiency, stability and scalability: A review. Mater. Sci. Energy Technol. 6, 437–459 (2023). https://doi.org/https://doi.org/10.1016/j.mset.2023.04.007

Khezzar, R., Zereg, M., Khezzar, A.: Modeling improvement of the four parameter model for photovoltaic modules. Sol. Energy. 110, 452–462 (2014). https://doi.org/https://doi.org/10.1016/j.solener.2014.09.039

Kotbi, A., Benyoussef, M., Ressami, E.M., Lejeune, M., Lakssir, B., Jouiad, M., Hills, V.: Gas Sensors Based on Exfoliated g-C 3 N 4 for CO 2 Detection. (2022)(a)

Kotbi, A., Imran, M., Kaja, K., Rahaman, A., Ressami, E.M., Lejeune, M., Lakssir, B., Jouiad, M.: Graphene and g-C_3N_4-Based Gas Sensors. J. Nanotechnol. 2022, 9671619 (2022)(b). https://doi.org/10.1155/2022/9671619

Langenhorst, M., Sautter, B., Schmager, R., Lehr, J., Ahlswede, E., Powalla, M., Lemmer, U., Richards, B.S., Paetzold, U.W.: Energy yield of all thin-film perovskite/CIGS tandem solar modules. Prog. Photovoltaics Res. Appl. 27, 290–298 (2019). https://doi.org/https://doi.org/10.1002/pip.3091

Lehr, J., Langenhorst, M., Schmager, R., Gota, F., Kirner, S., Lemmer, U., Richards, B.S., Case, C., Paetzold, U.W.: Energy yield of bifacial textured perovskite/silicon tandem photovoltaic modules. Sol. Energy Mater. Sol. Cells. 208, 110367 (2020). https://doi.org/https://doi.org/10.1016/j.solmat.2019.110367

Maniraj, B., Peer Fathima, A.: Parameter extraction of solar photovoltaic modules using various optimization techniques: a review. J. Phys. Conf. Ser. 1716, 12001 (2020). https://doi.org/10.1088/1742-6596/1716/1/012001

Montes-Romero, J., Almonacid, F., Theristis, M., de la Casa, J., Georghiou, G.E., Fernández, E.F.: Comparative analysis of parameter extraction techniques for the electrical characterization of multi-junction CPV and m-Si technologies. Sol. Energy. 160, 275–288 (2018). https://doi.org/https://doi.org/10.1016/j.solener.2017.12.011

Sarang, S.A., Raza, M.A., Panhwar, M., Khan, M., Abbas, G., Touti, E., Altamimi, A., Wijaya, A.A.: Maximizing solar power generation through conventional and digital MPPT techniques: a comparative analysis. Sci. Rep. 14, 8944 (2024). https://doi.org/10.1038/s41598-024-59776-z

Shell: Shell Solar Product Information Sheets, http://www.solarcellsales.com/techinfo/technical docs.cfm

Shen, K., Li, Q., Wang, D., Yang, R., Deng, Y., Jeng, M.-J., Wang, D.: CdTe solar cell performance under low-intensity light irradiance. Sol. Energy Mater. Sol. Cells. 144, 472–480 (2016). https://doi.org/https://doi.org/10.1016/j.solmat.2015.09.043

Smith, A.J., Meek, P.E., Liang, W.Y.: Raman scattering studies of SnS2 and SnSe2. J. Phys. C Solid State Phys. 10, 1321 (1977). https://doi.org/10.1088/0022-3719/10/8/035

Sriabisha, R., Hariharan, R.: High efficiency perovskite solar cell. Mater. Today Proc. 33, 450–453 (2020). https://doi.org/https://doi.org/10.1016/j.matpr.2020.05.031

Teixeira, C., Spinelli, P., Castriotta, L.A., Müller, D., Öz, S., Andrade, L., Mendes, A., Carlo, A. Di, Würfel, U., Wojciechowski, K., Forgács, D.: Charge Extraction in Flexible Perovskite Solar Cell Architectures for Indoor Applications – with up to 31% Efficiency. Adv. Funct. Mater. 32, 2206761 (2022). https://doi.org/https://doi.org/10.1002/adfm.202206761

Vais, R.I., Sahay, K., Chiranjeevi, T., Devarapalli, R., Knypiński, Ł.: Parameter Extraction of Solar Photovoltaic Modules Using a Novel Bio-Inspired Swarm Intelligence Optimisation Algorithm, (2023)

Wang, Z., Pang, F.: In-plane growth of large ultra-thin SnS2 nanosheets by tellurium-assisted chemical vapor deposition. RSC Adv. 7, 29080–29087 (2017). https://doi.org/10.1039/C7RA02599H

Xiao, H., Zhang, Y.C., Bai, H.: Molten salt synthesis of SnS2 microplate particles. Mater. Lett. 63, 809–811 (2009). https://doi.org/https://doi.org/10.1016/j.matlet.2009.01.010

Zhou, W., Umezawa, N.: Insight into the band structure engineering of single-layer SnS2 with in-plane biaxial strain. Phys. Chem. Chem. Phys. 18, 7860–7865 (2016). https://doi.org/10.1039/C6CP00039H